High dimensional approach to antiferromagnetic aperiodic spin systems

Sam Coates and Ryuji Tamura
Department of Materials Science and Technology,
Tokyo University of Science, 6 Chome–3–1 Niijuku, Katsushika City, Tokyo 125-8585

Monte Carlo approaches to aperiodic spin systems have found a range of antiferromagnetic ground states for both classical and quantum spins. In each case, the spin calculations have been undertaken on quasilattices in the appropriate dimension i.e. 1D for a Fibonacci chain, 2D for a Penrose tiling etc. Here we show that high dimension spin models can be calculated using the simplest of spin Hamiltonians, and that the projection of these high dimensional spins reproduces antiferromagnetic ground states in the 'correct' dimension. We also show a model for an atomistic antiferromagnetic quasicrystal, as derived using this method.

I. INTRODUCTION

Composition tuning of 'Tsai–type' quasicrystals and approximants has led to the discovery of intriguing properties in these complex systems, including novel quantum critical electronic properties [1–3] and superconductivity [4–6]. In particular, however, a rich array of magnetic transitions in simple and higher order approximants gives hope to finding an antiferromagnetic quasicrystal [7–11].

Aperiodic antiferromagnetic systems have been extensively studied theoretically in order to understand how aperiodicity affects magnetic long–range order. These works have considered both classical and quantum spins on aperiodic systems in 1, 2, and 3 dimensions under a range of Hamiltonians, often with complex interaction parameters to account for the changing bond lengths between adjacent spins [12–22]. In all cases, antiferromagnetic ground states were found.

Here, we present a simple model for exploring antiferromagnetic aperiodicity through a high–dimensional approach. To do so, we compute the spin ground–states of various high–dimensional lattices then use the projection method to study the resultant aperiodic spin structures. Therefore, there are two aims to this work: first, to show how previous theoretical works conducted in the 'appropriate' dimension can be represented and derived from a high dimensional approach. As a consequence, we show that a Monte Carlo calculated spin model can be computed in hyperspace using a simple Heisenberg Hamiltonian.

The second aim is to show an idealistic model of spins in an antiferromagnetic quasicrystal, using the same method used to produce the atomistic model of a Tsai–type quasicrystal. In this case we can use physically representative atomic distances to calculate the Fermi wave–vector (k_f) required for the Ruderman–Kittel–Kasuya–Yosida (RKKY) interaction to propagate antiferromagnetic order in such a material.

II. METHODS

Spins σ_i of dimensionality n were placed at the sites of n–dimensional lattices, where n = 2, 5, and 6. Their directions were randomised before normalization to unit length, i.e. their directions could form any point on an nD sphere. The Heisenberg Hamiltonian between the spins is:

$$E = -J \sum_{ij} \sigma_i \sigma_j \tag{1}$$

which was calculated for nearest (NN) and next–nearest neighbours (NNN) of spins. J was set to -1 and 1 for NN and NNN respectively, as for studying anti-ferromagnetic behaviour. In all dimensions, NN and NNN positions were calculated by the absolute distance between lattice points (i.e. NN = 1, NNN = $\sqrt{2}$). Likewise, for each system, periodic boundary conditions (PBCs) were applied.

The spin structure of each system was determined using the Metropolis–Hastings approach [23]. Temperatures of each system started at $k_{\mathrm{B}}\mathrm{T} = 3$, before stepping down logarithmically to 0.03 over 50 steps. Each lattice at each temperature was subjected to 10,000 Metropolis sweeps, which was determined to be enough calculation time to find sensible results i.e. magnetization per site $\rightarrow 0$. Subsequently, a final run of calculations was made with $k_{\mathrm{B}}\mathrm{T}$ stepping down from 1 to 0.01, after inserting the mean (opposing) spin directions at the relevant lattice sites. Again, each temperature was subjected to 10,000 Metropolis sweeps.

As n increases, the volume of space occupied by equivalent numbers of unit cells rapidly increases (i.e. c^n). To save calculation time, therefore, the number of points in lattices of n = 5, 6, were restricted to $3^5 = 243$ and $3^6 = 729$, respectively. In the 2D case, 11^2 lattice points and spins were used.

The projection method was used to obtain both the positions and spin vectors for each of the systems, with specific details provided within the results section. For

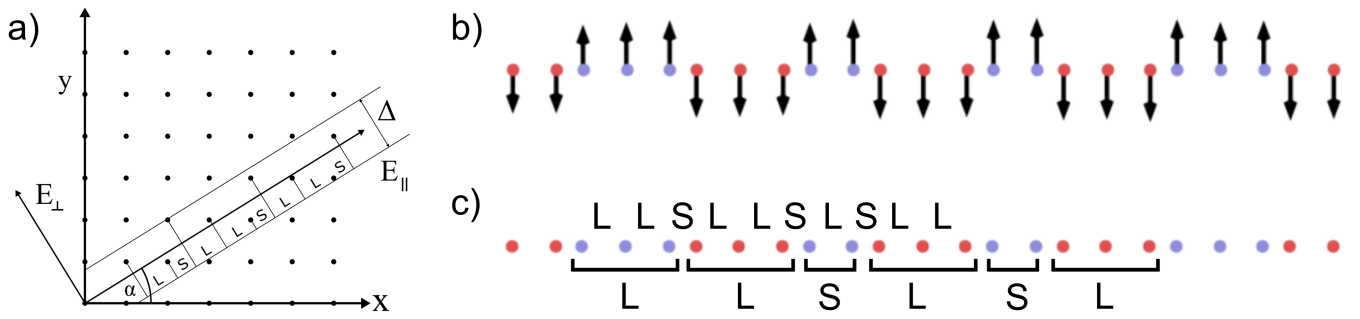

FIG. 1: (a) The projection method used to produce the Fibonacci chain. Parallel and perpendicular space are labelled as $E_{\parallel}$ and $E_{\perp}$ respectively. **(b)** The projected spin structure of the Fibonacci chain. Up and down spins are at positions coloured blue and red, respectively. **(c)** The hierarchical structure of the antiferromagnetic spins.

all cases, after projection into parallel space, the spin vectors were not normalized. This is to demonstrate the fact that their projected lengths are essentially equal, indicating that equilibrium was reached in higher dimensional space.

III. RESULTS AND DISCUSSION

Fibonacci Chain

The projection method for creating the Fibonacci chain has been discussed at length [24, 25]. Briefly, and shown in Figure 1(a), it involves overlaying an 'occupation domain' (OD) onto a 2D square lattice at an irrational angle α, where $\cot\alpha = \tau$. This window is of width $\Delta = a(\cos\alpha + \sin\alpha)$ where a is the lattice constant. The window consists of two sub–spaces, perpendicular (perp, $E_{\perp}$), and parallel (par, $E_{\parallel}$) space, where par–space is considered physical space. Lattice points inside the window are projected from perp–space onto par–space simply by setting their perp–space components to 0. This forms the Fibonacci chain.

After the spin calculation on the 2D lattice reaches its ground state, we can apply the same method: points which are inside the OD have their spin vector components projected onto par–space by setting their perp–space components to 0. As we are projecting onto 1D, their directions are parallel with the direction of the chain – therefore, to demonstrate the magnetic structure, we rotate the spin vectors by 90° after projection for clarity.

Figure 1(b) shows the result of the spin projection. Up spins have their positions coloured blue, down spins are red. In short, the magnetic structure can be described as ferromagnetic between L segments, and antiferromagnetic between S segments. This builds 'clusters' of either 2 or 3 ferromagnetic spins which can be grouped and separated by L or S segments, as demonstrated by Figure 1(c). Here, the spin arrows are removed and are simply represented by their colour. In this way, the spin chain is hierarchical. These findings are identical to those found in [12, 13], who placed spins on Fibonacci chains and calculated their ground state using sophisticated coupling components. Likewise, a similar projected spin structure of the Fibonacci chain was briefly discussed in [26].

Penrose Tiling

The projection method used for obtaining the Penrose tiling has also been well–documented, and was indeed one of the landmark examples of using higher dimensional space for structural analysis [27–29]. Essentially, if the perp–space components of a 5D lattice fall inside an occupation domain, then the par–space components of these points form the Penrose tiling. To perform the projection of the 5D points into either perp or par–space, a projection matrix is used which is formed of 5 orthonormal basis vectors, for example:

$$M = \begin{bmatrix} \cos(\frac{2\pi}{5}) & \cos(\frac{4\pi}{5}) & \cos(\frac{6\pi}{5}) & \cos(\frac{8\pi}{5}) & 1 \\ \sin(\frac{2\pi}{5}) & \sin(\frac{4\pi}{5}) & \sin(\frac{6\pi}{5}) & \sin(\frac{8\pi}{5}) & 0 \\ \cos(\frac{4\pi}{5}) & \cos(\frac{8\pi}{5}) & \cos(\frac{12\pi}{5}) & \cos(\frac{16\pi}{5}) & 1 \\ \sin(\frac{4\pi}{5}) & \sin(\frac{8\pi}{5}) & \sin(\frac{12\pi}{5}) & \sin(\frac{16\pi}{5}) & 0 \\ \sqrt{\frac{1}{2}} & \sqrt{\frac{1}{2}} & \sqrt{\frac{1}{2}} & \sqrt{\frac{1}{2}} & \sqrt{\frac{1}{2}} \end{bmatrix}$$

so that:

$$E_{\text{perp}} = \begin{bmatrix} M_3 \\ M_4 \\ M_5 \end{bmatrix} \tag{2}$$

$$E_{\text{par}} = \begin{bmatrix} M_1 \\ M_2 \end{bmatrix} \tag{3}$$

where perp– and par–space components of a 5D lattice can be calculated by the dot product of the lattice with equations (2) and (3) respectively. The occupation domain of the Penrose tiling, known as a rhombic icosahedron, is formed by the dot product of Eq. 2 with the 5D

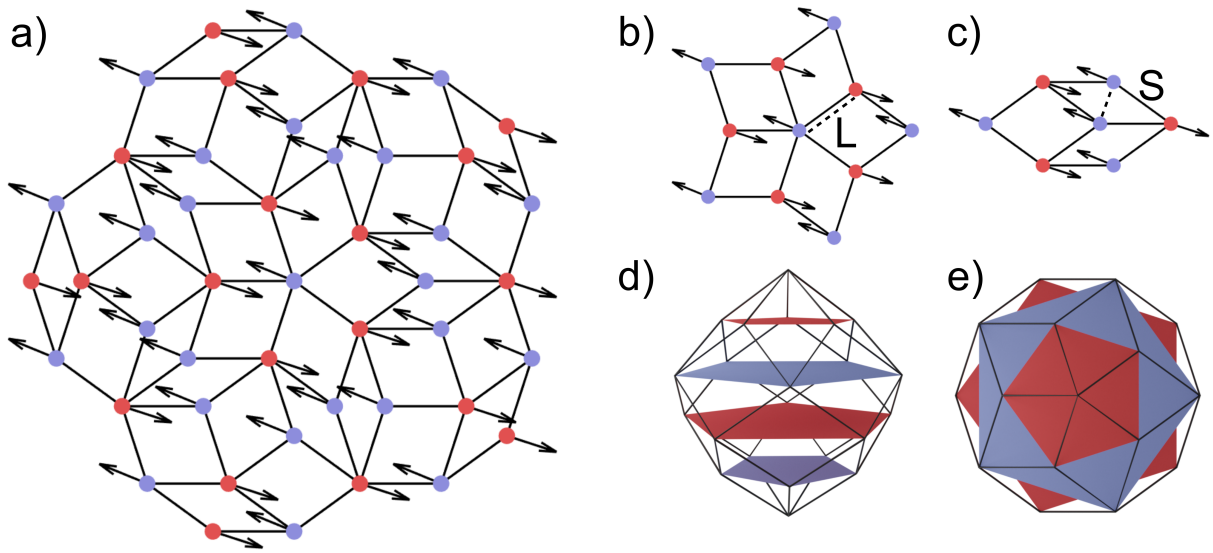

FIG. 2: **(a)** A section of the Penrose tiling decorated with projected spins. Again, 'up' spins are points coloured blue, 'down' are red. **(b)** An example of the NNN distance, where the dashed line indicates a large bond length between antiferromagnetic spins. **(c)** A NN distance S between two ferromagnetic spins. **(d)** The occupation domain used to produce the Penrose tiling, which can be partitioned for the two different spin lattices. **(e)** Top–down view of **(d)**.

unit cell. An example shown is in Figure 2(d), where the skeletal structure is the rhombic icosahedron. As with the Fibonacci chain example, the same technique can be used for the 5D spin vectors of the 5D lattice i.e. spins of points which fall into the occupation domain have their par–space components calculated using the dot product of the relevant spin vector with equation (3).

Figure 2(a) shows a section of the Penrose tiling obtained using the described method. Vertices are decorated with spin vectors which were obtained after projection from the 5D ground state. Each vertex is also coloured depending on the spin direction, where we describe red as 'down' and blue as 'up', although the spin direction is arbitrarily determined by the random nature of the Metropolis–Hastings algorithm.

There are two types of interactions on the tiling, dependent on two distances between spins. Examples are shown in Figure 2(b, c), where two vertices separated by L are antiferromagnetic (up–down), and those separated by S are ferromagnetic (up–up). This type of magnetic structure is therefore the same as derived for the Fibonacci chain i.e. NN is ferromagnetic, NNN is antiferromagnetic. Again, these results exactly match those obtained from anti–ferromagnetic spins on the Penrose tiling considering classical Hamiltonians [14–16].

We can also show that the up and down spin sites are populated on two specific sub–lattices, by showing the perp–space interpretation of their points. Here, we simply track where each spin/point originates from with respect to perp–space and the occupation domain. Figures 2(d, e) show the OD used to create the Penrose tiling, from a tilted perspective and top–down view respectively. Perp–space components of the 5D lattice which fall within the OD lie on one of the 4 coloured planes. The planes which create the up spin sites are coloured blue, and vice versa. In other words, each of the spin lattices are produced from specific cuts of perp–space.

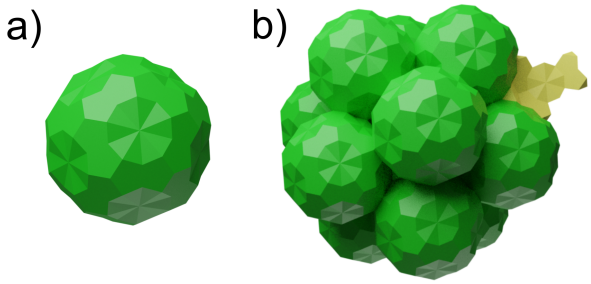

FIG. 3: **(a)** Archetype occupation domain used to build the larger occupation domains of the i–Cd–Yb model [30]. **(b)** Green: the total occupation domain used to produce the rare–earth icosahedra in the Tsai cluster. Yellow: part of the occupation domain which produces the rare–earth atoms in the AR units.

3D Atomistic Model

Similar to the Penrose tiling, the Amman–Beenker–Neri tiling [31] (or 3D Penrose) can be calculated using a 6D lattice. Again, we create a

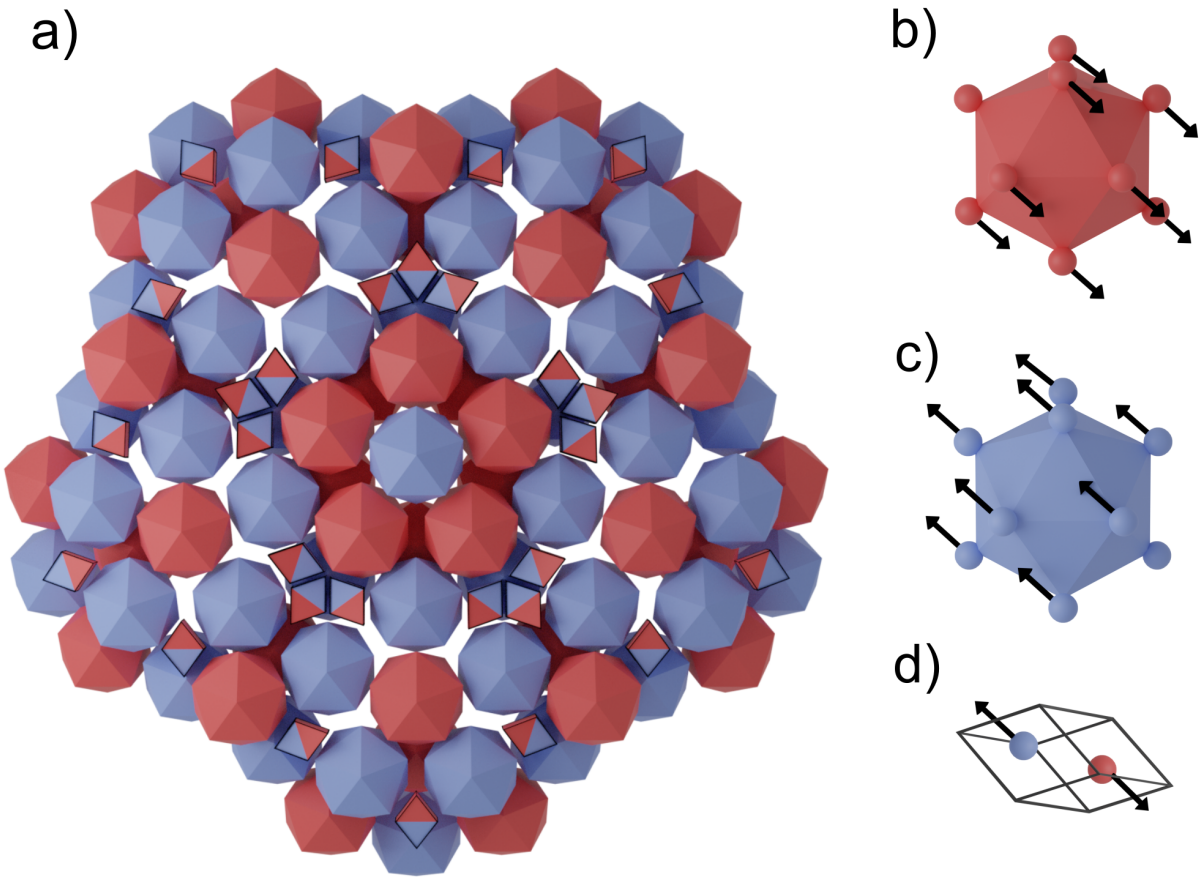

FIG. 4: **(a)** Slice of the 3D spin model. Each of the polyhedra represent groups of rare–earth atoms, which are coloured according to their spin. **(b)** A down spin icosahedra. **(c)** An up spin icosahedra. **(d)** The spins of the atoms contained within the AR unit.

projection matrix with orthonormal basis vectors:

$$M = \frac{a}{\sqrt{2+\tau}} \begin{bmatrix} 1 & \tau & \tau & 0 & -1 & 0 \\ \tau & 0 & 0 & 1 & \tau & 1 \\ 0 & 1 & -1 & -\tau & 0 & \tau \\ \tau & -1 & -1 & 0 & -\tau & 0 \\ -1 & 0 & 0 & \tau & -1 & \tau \\ 0 & \tau & -\tau & 1 & 0 & -1 \end{bmatrix}$$

so that:

$$E_{\text{perp}} = \begin{bmatrix} M_4 \\ M_5 \\ M_6 \end{bmatrix} \tag{4}$$

$$E_{\text{par}} = \begin{bmatrix} M_1 \\ M_2 \\ M_3 \end{bmatrix} \tag{5}$$

where a is the 6D lattice constant. An occupation domain (a rhombic triacontahedron) is formed in perp–space by the dot product of equation (4) and the 6D unit cell [32]. If the perp–space components of a 6D lattice fall within this occupation domain, then the corresponding par–space components of these points form the 3D Penrose tiling.

Here, however, we are interested in replicating the model which explains the structure of the Tsai–type group of quasicrystals, as a way of exploring the theoretical spin structure of a physical antiferromagnetic quasicrystal. In particular, the rare–earth atomic positions which would presumably carry the magnetic moment, as in the approximant samples [8–11] .

In this case, the occupation domain used is slightly more complex [30]. The OD which creates the 3D Penrose tiling is scaled down by τ^2, and its 5–fold vertices are truncated, as shown in Figure 3(a) – this aids in removing unphysically short atomic distances in the model [33]. This 'archetype' OD is then used to build a larger OD, which can be partitioned in perp–space to represent specific atomic constituents of the quasicrystal [30, 34].

Δ(Å)	J	Type
3.04	AFM	AR–ICO
3.52	FM	AR–AR
5.42	AFM	ICO_{inter}
5.70	FM	ICO_{intra}

TABLE I: Values of NN distances of rare–earth atoms taken from a scaled version of Figure 4(a). The type of magnetic interaction and which atoms are responsible are listed.

The occupation domain used to generate the rare–earth atom positions of the Tsai–type clusters in the *i*–Cd–Yb model is shown in Figure 3(b), where the archetype OD decorates an icosahedron. Shown in yellow is a section of the occupation domain which generates the rare–earth positions of the acute rhombohedra (AR) of the *i*–Cd–Yb model [30]. The AR block is unique to the higher order approximants and quasicrystals in the *i*–Cd–Yb family. Only one section is shown for clarity – the remaining sections occupy the 3–fold faces of the icosahedral OD.

As with the Penrose tiling, perp–space components of the 6D lattice which fall into the OD in Figure 3(b) have their positions and spins projected into par–space using equation 5. However, the number of rare–earth atom positions generated from the 3^6 lattice is only 24. Therefore, for analysing and presenting the real–space spin projections for the 6D system, the final equilibrium state was propagated in 6D under periodic boundary conditions before projection. This allows the generation of a large number of points and spins which represent the calculated ground state in 6D. For initial calculations we consider a as unity.

The real–space result of the projection is shown in Figure 4(a). This is a slice of the 3D model, perpendicular to one of the 5–fold axes. Rare–earth atoms are represented by the solid polyhedra they form, either icosahedra (i.e. those inside Tsai clusters) or acute rhombohedra (bordered in black). The polyhedra are coloured dependent on their spin, where the colours represent the ferromagnetic alignment of all spins on each icosahedron. Figure 4(b, c) shows the spin directions of all the atoms of individual icosahedra. Here we assign red as collectively 'down' and blue as collectively 'up' spin–icosahedra. Individual icosahedra are therefore ferromagnetic, with adjacent icosahedra showing opposing spin direction. The AR unit consists of two rare–earth atoms, with one up and one down spin, as shown in Figure 4(d).

This type of magnetic icosahedral–cluster structure is similar to the spin structure calculated for the antiferromagnetic 1/1 Au–Al–Gd approximant, which considers the RKKY interaction [35]. Experimentally, the 1/1 Au–Al–Tb approximant icosahedra show a more complex spin structure – here, individual icosahedra display a net magnetic moment of zero, manifested by a 'whirling' order along the [111] direction [9, 11]. In each case, adjacent icosahedra have opposing spin directions – a match with our calculations.

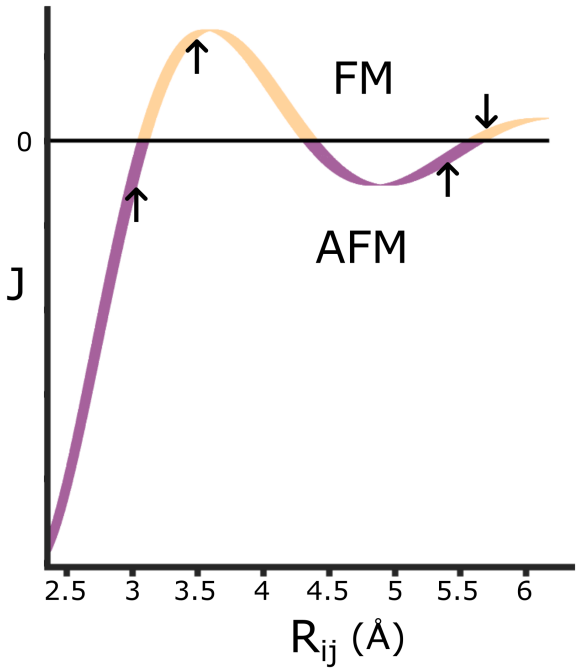

FIG. 5: The RKKY interaction calculated for the distances listed in Table I and iterative values of k_f. Arrows indicate the distances from Table I.

Both theoretically and experimentally, the total antiferromagnetic behaviour of the 1/1 approximants was discussed in terms of NN and NNN neighbour spins, i.e. antiferromagnetic interaction between NN sites, and ferromagnetic between NNN. We do the same here for the model in Figure 4(a), including the atomic positions of the AR unit. To do so, we scale the unit–size model so that atomic distances roughly match those experimentally observed in 2/1 approximants and quasicrystals. Table I shows the summary, where the type of magnetic interaction taken from Figure 4(a) is listed as either AFM or FM. The type of atom which contributes to these distances is also listed, where ICO is icosahedron, and intra/inter refers to atoms within icosahedra or adjacent icosahedra respectively.

The RKKY interaction:

$$J = \frac{-x\cos x + \sin x}{x^4} \tag{6}$$

where $x = 2k_f\Delta$ and k_f is the Fermi wave vector, was calculated for iterative values of k_f, to find the matching magnetic interactions for the corresponding distances listed in Table I. Figure 5 shows the resultant plot, for all $k_f = 1.23$–1.27 Å^{-1}. Arrows indicate the distances in Table I. These calculated values of k_f closely match with the values predicted to give antiferromagnetic order in the 1/1 Au–Al–Gd approximant [35], which considers k_f simply in terms of the Au concentration. In this case, the corresponding concentration values for Au would be: 93–85%, i.e. unfeasible values for a Tsai–type phase. However, of course, these values are dependent on the prescribed interatomic distances and the simplification of k_f. Smaller rare–earth distances and a more physical representation of k_f may give more realistic concentration values.

IV. CONCLUSIONS

The spin systems presented here represent ground states in their respective dimensions using a simplistic Hamiltonian. The projections are then geometric representations of these ground states in lower dimensions. The results produced for the 1 and 2 dimensional cases agree with all previous works which have used more complex interactions in the 'correct' dimension. The idealized 3 dimensional spin structure of a Tsai–type material was also presented, with potential paths to a real antiferromagnetic quasicrystal briefly discussed.

This work shows the basis of a toy model which can be used to compare with physical data of real quasicrystals. Likewise, the projected spins can act as a quick–start basis for further calculations in the correct dimension. Future work could include exploring the hyperspace models using different Hamiltonians, and exploring how non–unity spins have an effect on the magnetic ordering.

ACKNOWLEDGEMENTS

This work was supported by a Kakenhi Grant-in-Aid (No. 19H05817, 19H05818) from the Japan Society for the Promotion of Science (JSPS).

[1] K. Deguchi, S. Matsukawa, N. K. Sato, T. Hattori, K. Ishida, H. Takakura, and T. Ishimasa. Quantum critical state in a magnetic quasicrystal. *Nat. Mat.*, 11(12):1013–1016, 2012.

[2] T. Watanuki, S. Kashimoto, D. Kawana, T. Yamazaki, A. Machida, Yukinori Tanaka, and Taku J. S. Intermediate-valence icosahedral Au-Al-Yb quasicrystal. *Phys. Rev. B*, 86(9):094201, 2012.

[3] S. Jazbec, S. Vrtnik, Z. Jagličić, S. Kashimoto, J. Ivkov, P. Popčević, A. Smontara, H. J. Kim, J. G. Kim, and J. Dolinšek. Electronic density of states and metastability of icosahedral Au–Al–Yb quasicrystal. *Journal of Alloys and Compounds*, 586:343–348, 2014.

[4] K. Kamiya, T. Takeuchi, N. Kabeya, N. Wada, T. Ishimasa, A. Ochiai, K. Deguchi, K. Imura, and N. K. Sato. Discovery of superconductivity in quasicrystal. *Nat. Commun.*, 9(1):1–8, 2018.

[5] K. Deguchi, M. Nakayama, S. Matsukawa, K. Imura, K. Tanaka, T. Ishimasa, and N. K. Sato. Crystal structure of superconducting 1/1 cubic Au–Ge–Yb approximant with Tsai-type cluster. *Journal of the Physical Society of Japan*, 84(1):015002, 2015.

[6] K. Deguchi, M. Nakayama, S. Matsukawa, K. Imura, K. Tanaka, T. Ishimasa, and N. K. Sato. Superconductivity of Au–Ge–Yb approximants with Tsai-type clusters. *Journal of the Physical Society of Japan*, 84(2):023705, 2015.

[7] R. Tamura, Y. Muro, T. Hiroto, K. Nishimoto, and T. Takabatake. Long-range magnetic order in the quasicrystalline approximant cd 6 tb. *Phys. Rev. B*, 82(22):220201, 2010.

[8] A. Ishikawa, T. Hiroto, K. Tokiwa, T. Fujii, and R. Tamura. Composition-driven spin glass to ferromagnetic transition in the quasicrystal approximant Au-Al-Gd. *Phys. Rev. B*, 93(2):024416, 2016.

[9] A. Ishikawa, T. Fujii, T. Takeuchi, T. Yamada, Y. Matsushita, and R. Tamura. Antiferromagnetic order is possible in ternary quasicrystal approximants. *Phys. Rev. B*, 98(22):220403, 2018.

[10] S Yoshida, S Suzuki, T Yamada, T Fujii, A Ishikawa, and R Tamura. Antiferromagnetic order survives in the higher-order quasicrystal approximant. *Phys. Rev. B*, 100(18):180409, 2019.

[11] T. J. Sato, A. Ishikawa, A. Sakurai, M. Hattori, M. Avdeev, and R. Tamura. Whirling spin order in the quasicrystal approximant Au72 Al14 Tb14. *Phys. Rev. B*, 100(5):054417, 2019.

[12] H. Tsunetsugu and K. Ueda. Ising spin system on the Fibonacci chain. *Phys. Rev. B*, 36(10):5493, 1987.

[13] T. Tokihiro. Antiferromagnetic Heisenberg model on a quasiperiodic lattice with hierarchical interactions. *Phys. Rev. B*, 41(10):7334, 1990.

[14] J. Oitmaa, M. Aydin, and M. J. Johnson. Antiferromagnetic Ising model on the Penrose lattice. *Journal of Physics A: Mathematical and General*, 23(20):4537, 1990.

[15] D. Ledue, J. Teillet, J. Carnet, and J. Dujardin. Frustrated classical XY spin systems in the two-dimensional Penrose tiling. *Journal of non-crystalline solids*, 153:403–407, 1993.

[16] S. Matsuo, S. Fujiwara, H. Nakano, and T. Ishimasa. Long range antiferromagnetic order in Ising model simulations in a two-dimensional Penrose lattice. *Journal of non-crystalline solids*, 334:421–426, 2004.

[17] A. Jagannathan, A. Szallas, S. Wessel, and M. Duneau. Penrose quantum antiferromagnet. *Phys. Rev. B*, 75(21):212407, 2007.

[18] A. Koga and H. Tsunetsugu. Antiferromagnetic order in the Hubbard model on the Penrose lattice. *Phys. Rev. B*, 96(21):214402, 2017.

[19] S. Wessel, A. Jagannathan, and S. Haas. Quantum antiferromagnetism in quasicrystals. *Phys. Rev. Lett.*, 90(17):177205, 2003.

[20] E. Y. Vedmedenko, U. Grimm, and R. Wiesendanger. Noncollinear magnetic order in quasicrystals. *Phys. Rev. Lett.*, 93(7):076407, 2004.

[21] U. Grimm and M. Baake. Aperiodic Ising models. *arXiv preprint cond-mat/9604116*, 1996.

[22] S. Matsuo, T. Ishimasa, and H. Nakano. Antiferromagnetic orders in Ising model simulations in an icosahedral Zn–Mg–Ho structure. *Materials Science and Engineering: A*, 294:633–637, 2000.

[23] S. Chib and E. Greenberg. Understanding the metropolis-hastings algorithm. *The American Statistician*, 49(4):327–335, 1995.

[24] C. Janot. Quasicrystals: A primer. *Monographs on the Physics and Chemistry of Materials, Oxford University Press, Oxford*, 1992.

[25] Françoise Axel, Françoise Dénoyer, and Jean Pierre Gazeau. *From Quasicrystals to More Complex Systems: Les Houches School, February 23–March 6, 1998*, volume 13. Springer Science & Business Media, 2013.

[26] T. J Sato, Hiroyuki Takakura, An Pang Tsai, Kaoru Shibata, Kenji Ohoyama, and Ken H Andersen. Antiferromagnetic spin correlations in the Zn-Mg-Ho icosahedral quasicrystal. *Physical Review B*, 61(1):476, 2000.

[27] N. G. de Bruijn. Algebraic theory of Penrose's non-periodic tilings of the plane. *Kon. Nederl. Akad. Wetensch. Proc. Ser. A*, 43(84):1–7, 1981.

[28] N. G. De Bruijn. Quasicrystals and their Fourier transform. *Indagationes Mathematicae*, 89:123–152, 1986.

[29] F. Gahler and J. Rhyner. Equivalence of the generalised grid and projection methods for the construction of quasiperiodic tilings. *Journal of Physics A: Mathematical and General*, 19(2):267, 1986.

[30] H. Takakura, C. P. Gómez, A. Yamamoto, M. de Boissieu, and A. P. Tsai. Atomic structure of the binary icosahedral Yb–Cd quasicrystal. *Nat. Mater.*, 6(1):58, 2007.

[31] P. Kramer and R. Neri. On periodic and non-periodic space fillings of Em obtained by projection. *Acta Crystallographica Section A: Foundations of Crystallography*, 40(5):580–587, 1984.

[32] W. Steurer and J. Dshemuchadse. *Intermetallics: structures, properties, and statistics*, volume 26. Oxford University Press, 2016.

[33] M. de Boissieu, H. Takakura, C. P. Gòmez, A. Yamamoto, and A. P. Tsai. Structure determination of quasicrystals. *Philosophical Magazine*, 87(18-21):2613–2633, 2007.

[34] T. Yamada, H. Takakura, M. De Boissieu, and A. P. Tsai. Atomic structures of ternary Yb–Cd–Mg icosahedral quasicrystals and a 1/1 approximant. *Acta Crystallographica Section B: Structural Science, Crystal Engineering and Materials*, 73(6):1125–1141, 2017.

[35] H. Miyazaki, T. Sugimoto, K. Morita, and T. Tohyama. Magnetic orders induced by RKKY interaction in Tsai-type quasicrystalline approximant Au-Al-Gd. *Phys. Rev. Mater.*, 4(2):024417, 2020.